THE JOURNAL OF PHYSICAL CHEMISTRY B

Article

pubs.acs.org/JPCB

# Effect of Urea Concentration on Aggregation of Amyloidogenic Hexapeptides (NFGAIL)

Zhuowei Cai,[‡,†] Jingqiang Li,[‡,†] Chunji Yin,[‡] Zaixing Yang,[‡,§,*] Jianlan Wu,[‡,⊥,*] and Ruhong Zhou[⊥,∥]

[‡]Department of Physics, Zhejiang University, Hangzhou, 310027, China

[§]Department of Engineering Mechanics, Zhejiang University, Hangzhou 310027, China

[⊥]Soft Matter Research Center, Zhejiang University, Hangzhou 310027, China

[∥]Computational Biology Center, IBM Thomas J. Watson Research Center, Yorktown Heights, New York 10598, United States

Supporting Information

**ABSTRACT:** We have performed large-scale all-atom molecular dynamics (MD) simulations to study the aggregation behavior of four NFGAIL hexapeptides in the aqueous urea solution, with a urea concentration ranging from 0 to 5 M. We find that urea in general suppresses the peptide aggregation, but suppression slows down in the intermediation concentration regime around 3 M. Two competing mechanisms of urea are determined: urea molecules accumulated near the first solvation shell (FSS) tend to unfold the hexapeptide, which favors aggregation; on the other hand, the tight hydrogen bonds formed between urea and peptide mainchains hinder the association of peptides which disfavors the formation of the $\beta$-sheet. Furthermore, the different nonlinear urea concentration dependences of the urea−peptide and peptide−peptide hydrogen bonds lead to a nonmonotonic behavior, with a weak enhancement in the peptide aggregation around 3 M.

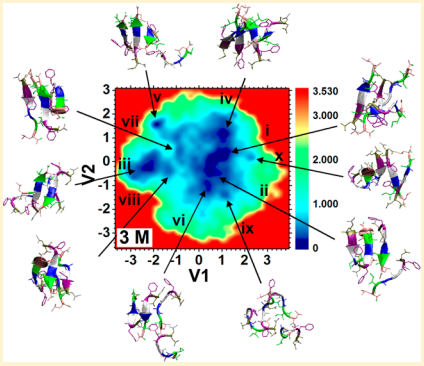


## INTRODUCTION

A large number of protein conformational diseases such as type II diabetes,[1,2] Alzheimer's disease (AD),[3−5] and cataracts,[6] are directly associated with protein misfolding and the subsequent amyloidogenesis. A misfolded protein usually exhibits a more extended configuration than its native structure. Recent evidence shows that partially ordered oligomers formed in the early aggregation stage of misfolded proteins are major cytotoxic agents to the living cell, and the aggregation process itself is also found cytotoxic.[7−15] These small oligomers can be nucleation seeds for the subsequent large-scale amyloidogenesis. Experimental results have demonstrated that, under suitable external conditions (e.g., urea concentration, pH, salt concentration, and temperature), many common proteins can also form ordered amyloid fibrillar aggregates.[16] Therefore, it is crucial to understand molecular mechanisms of key external triggers for proteins misfolding and the related aggregation.

As a strong denaturant for proteins,[17] urea has been widely used in *in vitro* unfolding/refolding experiments.[18−50] Urea can directly attack protein mainchains and side chains, rather than indirectly disrupt the water structure as a "water breaker".[29−37,43,51−53] The denaturing power of urea mainly comes from a stronger dispersion interaction between urea and proteins over water and proteins.[43,52] In urea, a globular native protein often becomes fully or partially unfolded, exhibiting a more extended and open structure. The similar behavior is observed for small unstructured poly peptides. Stretched protein monomers in urea are favored for the subsequent aggregation and fibrillization. On the other hand, in order to form an ordered aggregate (i.e., a $\beta$-sheet), the protein−protein interactions have to compete with the hydrogen bonding formation in urea-protein interactions, which can slow down the aggregation process in urea. These two different behaviors imply that urea can affect the protein aggregation process in a complicated way, leading to rich phenomena.

Dobson and co-workers[54] experimentally studied the urea effect on aggregation of a globular protein, $\beta$-lactoglobulin. A nonmonotonic dependence on urea concentration is observed for the protein aggregation, with a maximum rate occurring near 5 M, where an elaborate balance is built between promoting aggregate-prone monomers and inhibiting interpeptide interactions. This phenomenon is consistent with the theoretical prediction based on the kinetic partitioning mechanism for monomeric protein folding.[55,56] Furthermore, it is interesting to investigate whether this nonmonotonic phenomenon exists for the aggregation of short poly peptides, which is more easily extended from its initial random-coil structure than a compact globular protein. Thirumalai and co-workers[34] made an important initial exploration about the urea effect on the aggregation of A$\beta_{16-22}$ (KLVFFAE) peptides. Their simulation shows that the trimeric $\beta$-sheet is severely destabilized in 8 M urea, while monomers are effectively stretched. Combining experiments of Dobson and co-workers, Thirumalai and co-workers speculated that an optimal urea

**Received:** August 4, 2013
**Revised:** December 11, 2013
**Published:** December 11, 2013

   dx.doi.org/10.1021/jp407776e | J. Phys. Chem. B 2014, 118, 48−57

concentration might exist for short poly peptides to display a maximal rate of amyloidogenesis. However, a thorough study on the dependence of the aggregation of short poly peptides with urea concentrations is still nonexistent.

To address the above concerns, we have investigated the aggregation of NFGAIL peptides in various urea concentrations in this paper. NFGAIL peptide is the core and the shortest amyloidogenic segment of human islet amyloid polypeptide ($hIAPP_{22-27}$), which is directly related to type II diabetes mellitus.[1,2] Many experiments and simulations have shown that the aggregation dynamics of NFGAIL is very similar to that of the full hIAPP peptide and also exhibits cytotoxicity to islet cells.[1,40−43] In our study, large-scale all-atom molecular dynamics (MD) simulations are applied to explore the aggregation behavior of four NFGAIL hexapeptides in the aqueous urea solution. With extensive simulations and analyses for different urea concentrations, we expect to reveal the detailed and complex role of urea on the aggregation of short poly peptides, which might help better understand the denaturing power of urea.

## METHOD AND MODELS

We perform large-scale all-atom molecular dynamics (MD) simulations to comparatively study the aggregation behavior of four NFGAIL hexapeptides in the urea solution with 13 different concentrations (ranging from 0 to 5 M, with 0.5 M increment, and two additional concentrations at 2.7 and 3.2 M for local data enhancement, see Table 1 for details).

**Table 1. Summary of the Simulation Information**

| concentration of urea solution (M) | no. of urea molecules | no. of water molecules | initial simulation box size (nm × nm × nm) |
|---|---|---|---|
| 0.0 | 0 | 3512 | 4.82 × 4.82 × 4.82 |
| 0.5 | 31 | 3372 | 4.79 × 4.79 × 4.79 |
| 1.0 | 60 | 3361 | 4.81 × 4.81 × 4.81 |
| 1.5 | 92 | 3254 | 4.79 × 4.79 × 4.79 |
| 2.0 | 124 | 3114 | 4.78 × 4.78 × 4.78 |
| 2.5 | 157 | 3022 | 4.77 × 4.77 × 4.77 |
| 2.7 | 175 | 2961 | 4.74 × 4.74 × 4.74 |
| 3.0 | 194 | 2919 | 4.75 × 4.75 × 4.75 |
| 3.2 | 209 | 2852 | 4.76 × 4.76 × 4.76 |
| 3.5 | 214 | 2845 | 4.74 × 4.74 × 4.74 |
| 4.0 | 257 | 2740 | 4.73 × 4.73 × 4.73 |
| 4.5 | 289 | 2616 | 4.72 × 4.72 × 4.72 |
| 5.0 | 323 | 2534 | 4.72 × 4.72 × 4.72 |

In this study, MD simulations are performed with the GROMACS-4.0.7 package.[57] VMD software[58] is used to visualize/analyze trajectories and draw molecular pictures. The OPLSAA force field,[59] SPC water model,[60] and OPLS urea model[61,62] are employed for the NFGAIL peptide, explicit water solvent, and urea, respectively. Long-range electrostatic interactions are treated with particle-mesh Ewald (PME) method,[4] and a typical 12 Å cutoff is applied for van der Waals (vdW) interactions. The LINCS algorithm[63] is applied to constrain bond lengths of all bonds within peptides and urea, while the SETTLE algorithm[64] is applied to constrain the bond lengths and angles in water. The simulation temperature are maintained at 310 K using Berendsen's algorithm[65] with a coupling constant of 0.2 ps.

A monomeric NFGAIL peptide is taken from the Protein Data Bank (PDB ID 2KIB)[66] and capped with acetyl (N-terminal) and amide (C-terminal) groups for neutralization. This peptide is placed into a water box and simulated at 310 K with an NVT ensemble for 10 ns. Then, a compact random-coil peptide is extracted from the simulation trajectory as the initial structure for subsequent aggregation simulations. In the aggregation simulations, four unstructured peptides are randomly immersed in a water or pre-equilibrated urea−water mixture box, following our previous protocols,[67−71] with a minimum separation of at least 1.5 nm from each other to avoid artificial effects (see Figure 1, using the pure water and 3.0 M urea systems for demonstration). Table 1 summarizes the detailed simulation information, including box size, and numbers of urea and water molecules, for each urea concentration. The mixture systems are equilibrated with a 2000-step (4 ps) conjugate gradient minimization at 310 K. Then, a position restrained simulation (with all the heavy atoms on the peptides restrained) is performed to fully equilibrate the solvent for 2 ns. Then, 10 independent configurations are extracted from the above position-restrained simulation trajectory as the starting conformations for the following aggregation simulations. For each concentration, 10 independent 200 ns long simulation trajectories are generated for data collection with the *NPT* ensemble (at 300 K and 1 atm, both constant temperature and constant pressure are controlled by the Berendsen methods,[65] with a coupling constant of 0.2 ps for thermostat and 20 ps for barostat). A time step of 2 fs is used for each trajectory. The total aggregated simulation time for this study is about 26 $\mu$s.

## RESULTS

**Nonmonotomic Peptide Aggregation with the Increase of Urea Concentration.** The aggregation simulations of four NFGAIL peptides are performed in the aqueous urea solutions ranging from 0.0 to 5.0 M. To identify the structural distribution and capture relevant configurations of oligomers from a vast conformational space sampled by ten independent 200 ns trajectories, we apply the dihedral principal components analysis (dPCA) along peptide backbone dihedral angles.[72−77] Two-dimensional free energy surfaces for oligomers were projected onto the first two eigenvectors, V1 and V2, of the dPCA. Basins in the free energy landscape usually correspond to oligomer conformations with more appearances during the peptide aggregation process.

Parts A−D of Figure 2 show the free energy landscapes of oligomers sampled from all the simulations in the pure water, 2.0, 3.0, and 5.0 M urea, respectively. In the pure water (see Figure 2A), many basins are away from the point of origin in the conformational space. We extract the representative configurations for the 10 most possible basins and found a remarkable heterogeneity in secondary structures. Compared to unstructured oligomers at the point of origin, oligomers in most of other basins are ordered, forming a dimeric or trimeric $\beta$-sheet, the latter with a larger population. The peptide arrangement within the $\beta$-sheets is also flexible. The $\beta$-sheets in basins ii, iii, ix, and x are antiparallel; while those in basins iv and v are parallel. Interestingly, the $\beta$-sheets in basin vi and vii are hybrid with both parallel and antiparallel orientations. Relatively speaking, the antiparallel $\beta$-sheets are more populated. For an ideal in-register antiparallel NFGAIL $\beta$-sheet, the detailed residual registration between two paired peptides is Asn22-Leu27, Phe23-Ile26, Gly24-Ala25, Ala25-Gly24, Ile26-Phe23, and Leu27-Asn22, where residues before and after dash are from the first and second peptides,


dx.doi.org/10.1021/jp407776e | J. Phys. Chem. B 2014, 118, 48−57

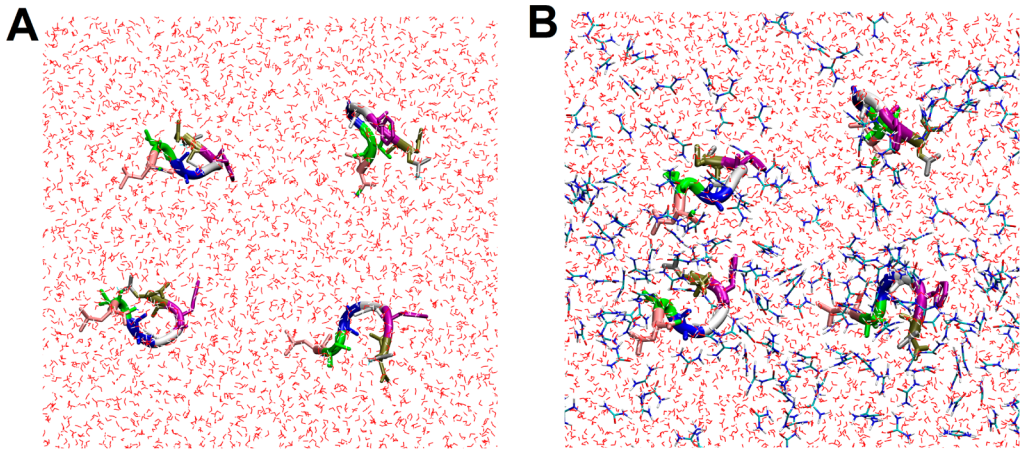


**Figure 1.** Initial random-coil configurations of NFGAIL peptides for the simulations in (A) pure water, and (B) 3.0 M urea as an example. The peptides are shown with the new cartoon, water molecules with red wires, urea with bold bonds. Each residue is in a different color: Asn22 in yellow, Phe23 in purple, Gly24 in white, Ala25 in blue, Ile26 in green, and Leu27 in pink.

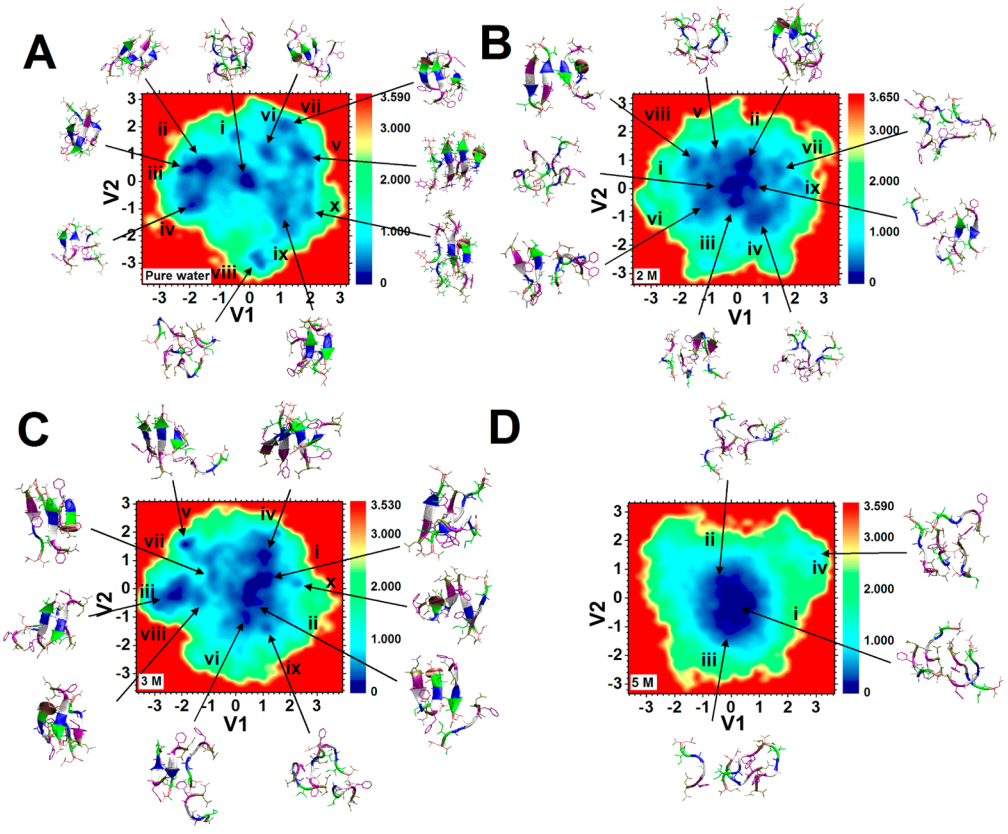


**Figure 2.** Projection of the free energy surface for NFGAIL oligomers in terms of the two lowest eigenvectors of the dPCA, obtained from 10 independent 200 ns trajectories for each urea concentration: (A) pure water, (B) 2.0 M, (C) 3.0 M, and (D) 5.0 M. The scale for the free energy (in kcal/mol) is given on the right panel of each figure. For all the free energy surfaces, a typical configuration is presented with an arrow connected with each free energy basin.

respectively. For an ideal in-register parallel NFGAIL $\beta$-sheet, each residue of the first peptide is hydrogen bonded with the same residue of the second peptide. In our simulation in water and urea solutions, the parallel $\beta$-sheets usually follow the residual registration, while the antiparallel $\beta$-sheets are guided by the residual registration but allow flexibility of one or two sites mismatching (see Figure 2 and Figure S1 of the Supporting Information for residual color matching).

As the urea concentration increases to 2.0 M (see Figure 2B), the oligomer conformations become less distributed, and only a few weaker basins are away from the point of origin. Compared to Figure 2A, oligomers become less compact and peptides become more extended. The content of disordered oligomers is largely increased, at the expense of losing secondary structures. We observe that two or three peptides form the antiparallel $\beta$-sheets for oligomers in basins iii, vi, viii, and ix, while two peptides form the parallel $\beta$-sheet in basin ii. The decrease of


dx.doi.org/10.1021/jp407776e | J. Phys. Chem. B 2014, 118, 48−57

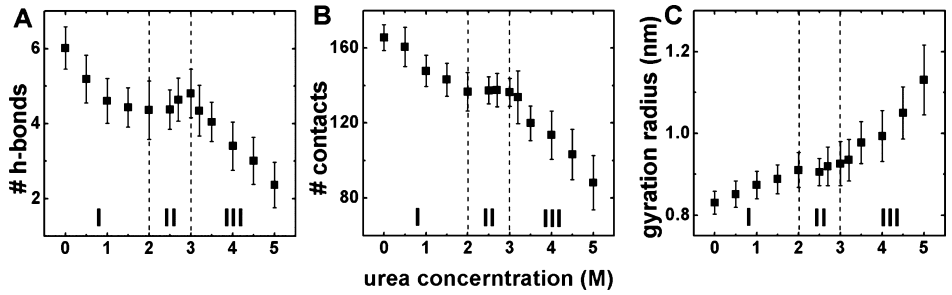


**Figure 3.** Three quantities measuring the aggregation extent (50−200 ns) in different urea concentrations: (A) the number of hydrogen bonds between all peptide mainchains, (B) the average contact number of heavy atoms between all pairs of peptides, and (C) the gyration radius. The error bars are the standard errors about the means.

ordered structures indicates the suppression of the peptides aggregation by the urea solution.

With a further increase of the urea concentration up to 3.0 M (see Figure 2C), free energy basins far away from the point of origin reappear. We calculate representative oligomer configurations for the nine most possible basins. Compared to simulations at 2.0 M shown in Figure 2B, the number of ordered structures is increased: two or three peptides form the antiparallel $\beta$-sheets in basins i, ii, iii, vi, vii, and viii, and the $\beta$-sheets in basin vi, v and x are hybrid with both parallel and antiparallel orientations. However, as the urea concentration continues increasing above 3.0 M, the urea inhibition gradually dominates for the $\beta$-sheet aggregation. The free energy landscape in Figure 2 D shows that the oligomer is almost completely unstructured with extended but spatially separated monomers at 5.0 M urea. Overall, we observe that urea can suppress the aggregation of NFGAIL peptides, but a nonmonotonic behavior is observed in the intermediate urea concentration regime (more discussions below).

**The Slow-Down of Urea Suppression at Moderate Urea Concentrations.** To further probe the urea effect on the aggregation of NFGAIL peptides demonstrated above, three quantities are calculated to evaluate the simulation results from different perspectives, that is, the number of hydrogen bonds between all pairs of peptide mainchains, the average contact number of heavy atoms between all pairs of peptides, and the radius of gyration for the whole oligomer. For each concentration, the time evolution of these three quantities is recorded by averaging over all the ten trajectories. The data from 50 to 200 ns are used for the further statistical averages, which will be first discussed below. These three quantities from oligomers formed in our simulations, as compared with results of an ideal $\beta$-sheet, can provide a good understanding on the peptide aggregation behaviors. The ideal $\beta$-sheet formed by four peptides can exhibit a single-layer structure or a double-layer structure with each layer containing two peptides. Here we first explore the ideal single-layer and double-layer $\beta$-sheets based on the NFGAIL fibrillar crystal structure deposited on the Protein Data Bank (PDB ID 2KIB).[66] For one $\beta$-sheet, the numbers of hydrogen bonds between peptide mainchains are 12 (single-layer) and 8 (double-layer), the average contact numbers of heavy atoms between all pairs of peptides are 140 (single-layer) and 106 (double-layer), and the gyration radius for the full oligomer is 0.92 nm (both single-layer and double-layer). Notice that hydrophobicity can lead to a less-structured but compact oligomer of NFGAIL peptides. Consequently, the heavy atom contact number and the gyration radius of the ideal $\beta$-sheet may not be necessarily the upper and lower limits of our calculations, respectively.

We first investigate the number of hydrogen bonds formed between all the pairs of mainchains, which can reflect the orderliness of the oligomer. Here, a hydrogen bond is considered to be formed if the distance between a donor and an acceptor is less than 3.5 Å and the donor-hydrogen-acceptor angle is larger than 150°. As shown in Figure 3A, we find that the hydrogen bond number consistently and quickly decreases from 6.0 in the pure water to 4.4 in 2.0 M urea (regime I). Interestingly, the hydrogen bond number then slowly increases from 4.4 to 4.8, as the urea concentration increases from 2.0 to 3.0 M (regime II). As the urea concentration further increases from 3.0 M (regime III), the hydrogen bond number decreases sharply to 2.4 in 5.0 M urea. A local maximum hydrogen bond number is observed at ∼3.0 M urea, which suggests the possibility of a partial enhancement for the NFGAIL aggregation around 3.0 M.

Figure 3B presents the average contact number of heavy atoms between all peptide pairs as the function of the urea concentration. This quantity indicates the geometric structure of the oligomer. Here, two heavy atoms, from any two different peptides, are considered to be contacted when their distance is less than 6.0 Å. Similar to the hydrogen bond number, the average contact number of heavy atoms between all peptide pairs generally decreases with the urea concentration but in a nonmonotonic way: this number decreases from 166 in the pure water to 137 in 2.0 M urea (regime I), remains nearly unchanged in regime II, and then dramatically decreases to 88 in 5.0 M urea (regime III). The absolute value of the heavy atom contact number between all pairs of peptides can be larger than the limit from the ideal $\beta$-sheet, possible due to compact but less-structures oligomers as we discussed.

The compactness of the oligomer can also be viewed by the radius of gyration, which increases as the oligomer becomes swelled. As shown in Figure 3C, the gyration radius increases from 0.83 nm in the pure water to 0.91 nm in 2.0 M urea (regime I), and this spatial extension indicates a gradually destabilized trend of the $\beta$-sheet together with the dPCA in Figure 2. In the regime II from 2.0 to 3.0 M, the gyration radius is almost unchanged at 0.91−0.92 nm. With a continued extension of peptides, the overall radius of the oligomer is held by the small enhancement of the $\beta$-sheet, as shown by the configurations in Figure 2C. When the urea concentration further increases from 3.0 M (regime III), the gyration radius sharply increases to 1.13 nm in 5.0 M urea, which suggests that the oligomer is swelled and the ordered $\beta$-sheet is unfavored.


dx.doi.org/10.1021/jp407776e | J. Phys. Chem. B 2014, 118, 48−57

The results of the three above quantities, the hydrogen bond number of all peptide pairs, the average heavy atom contact number between all peptide pairs, and the gyration radius, are in excellent accordance. Each quantity is a nonmonotonic function of the urea concentration. Three urea concentration regimes, I (0.0 M ∼ 2.0 M), II (2.0 M ∼ 3.0 M), and III (>3.0 M), distinguish three behaviors of the $\beta$-sheet formation. Combining with the dPCA in Figure 2, our simulation results show that the urea in general suppresses the aggregation of NFGAIL peptides, but suppression slows down in the intermediate urea concentration regime around 3.0 M and the formation of the $\beta$-sheet can be partially enhanced.

**Influence of Urea on Peptide Mainchains and Side Chains during Aggregation.** To further understand the aggregation process of NFGAIL peptides in urea solutions, we explore two of the above structural quantities in more detail to identify different contributions.

As the first step, we use the heavy atom contact number to distinguish the influences on peptide mainchains and side chains from urea. With respect to the location of two contacted heavy atoms, the total contact number can be written as a sum of three components: main chain−main chain (mc−mc), side chain−side chain (sc−sc), and main chain−side chain (mc−sc). As shown in Figure 4, each component behaves similarly and

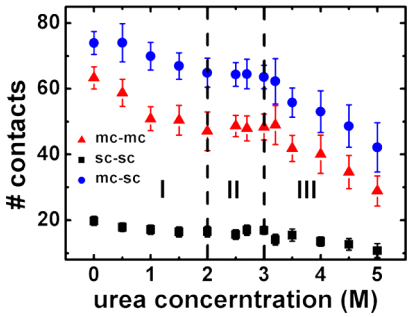


**Figure 4.** The three components of heavy atom contact numbers (50−200 ns), including main chain−main chain (mc−mc, red), side chain−side chain (sc−sc, black), and main chain-side chain (mc−sc, blue), with the change of urea concentrations. The error bars are the standard errors about the means.

can be categorized into the three urea concentration regimes (I, 0.0−2.0 M; II, 2.0−3.0 M; III, >3.0 M) introduced above. In regime I, the heavy atom contact numbers of mc−mc, mc−sc, and sc−sc consistently decrease from 63 to 47, from 74 to 65, from 20 to 17, respectively. In regime II, these three contact numbers are either weakly increased (from 47 to 48 for mc−mc) or almost unchanged (64 for mc−sc and 17 for sc−sc). In regime III, the contact numbers of mc−mc, mc−sc, and sc−sc experience a fast decrease, eventually becoming 29, 43, and 11 in 5.0 M urea, respectively. In the urea solution, urea molecules are accumulated in the first solvation shell (FSS) of NFGAIL mainchains and side chains by different driving forces. Since the NFGAIL is a highly hydrophobic peptide with only one polar Asn22 side chain, urea molecules are attracted to the side chains mainly by their stronger dispersion interactions than water, whereas additional tighter hydrogen bonds can be formed between urea molecules and mainchains. The association between urea and mainchains directly competes with the peptide aggregation, which will be illustrated by the following analysis of hydrogen bonds. The interplay between mainchains and side chains, however, results in similar behaviors with the change of the urea concentration.

Next we study the time evolution of the three types of contact number. As a demonstration, we present results of four typical urea concentrations (0.0, 2.0, 3.0, and 5.0 M) in the left panels of Figure 5. Here the log scale for the time axis illustrates dynamics in different time ranges. For all the simulations, the side chains appear to contact earlier than the mainchains. Around 1 ns, the mainchains become active and both the mc−mc and mc−sc contact numbers increase quickly, exceeding the sc−sc contact number. The fast growth of mc−mc and mc−sc contact numbers in general starts later in the urea solutions (>1 ns) than in the pure water (<1 ns), due to urea accumulation near the FSS of mainchains. All the three contract numbers are rescaled by their maximum values to be reduced contact ratios. From the contact ratios in the right panels of Figure 5, we find that the relative time dependences of all the three contact numbers share similarities. Through almost the same time scale, we observe "kinks" from the spatial adjustment along the curves of contact numbers. For three different contact ratios, these kinks are often correlated, so that the conformational changes of main chains and side chains affect each other, especially at long times. The appearance of these kinks is consistent with hydrogen bonding dynamics discussed later in this paper. The mainchains and side chains of NFGAIL peptides thus play different roles in the aggregation process.[78−80] The hydrophobic side chains drive the initial association of peptides. With a jointed effort from side chains, mainchains are adjusted spatially later to promote hydrogen bonds, which are crucial for the final formation of an ordered oligomer, e.g., $\beta$-sheet.[78,80]

**Competing Mechanism for the Peptide Aggregation.** The formation of stable hydrogen bonds between peptide mainchains (mc−mc) is a crucial step of fibrillization. In aqueous urea solution, the amide proton of the peptide mainchains can also form hydrogen bonds with oxygen of water (water−mc) and carbonyl oxygen of urea (urea−mc). The competition from these three different types of hydrogen bonds determines the configuration of the aggregated oligomer. The numbers of mc−mc, water−mc, and urea−mc hydrogen bonds are plotted as the function of the urea concentration in Figure 6A. Water molecules are gradually replaced by urea molecules in the simulation box as the urea concentration increases (see Table 1), so that the number of water−mc hydrogen bonds decreases along with the increase in the number of urea−mc hydrogen bonds. More importantly, the accumulation of urea molecules in the FSS can extend the NFGAIL monomer and more hydrogen-bonding sites are exposed in the NFGAIL mainchains. From the pure water to 5.0 M urea, the increment of the urea−mc hydrogen bonds is about twice the decrement of the water−mc hydrogen bonds.

Because of the incompatible polarity between water and NFGAIL peptides, the NFGAIL monomer usually adopts a compact random-coil structure in the pure water, which harbors hydrogen bonding sites inside the collapsed structure. On the other hand, both the mc−mc and the urea−mc hydrogen bonds are more pronounced for extended peptides. To better understand the "stretchiness" of the NFGAIL peptides, we compute the partial summation of mc−mc and urea−mc hydrogen bond numbers. As shown in Figure 6B, the number of the "stretched" hydrogen bonds (urea−mc + mc−mc) consistently increases with the urea concentration, indicating that the NFGAIL peptides become more extended due to the increment of urea molecules. However, small urea molecules


dx.doi.org/10.1021/jp407776e | J. Phys. Chem. B 2014, 118, 48−57

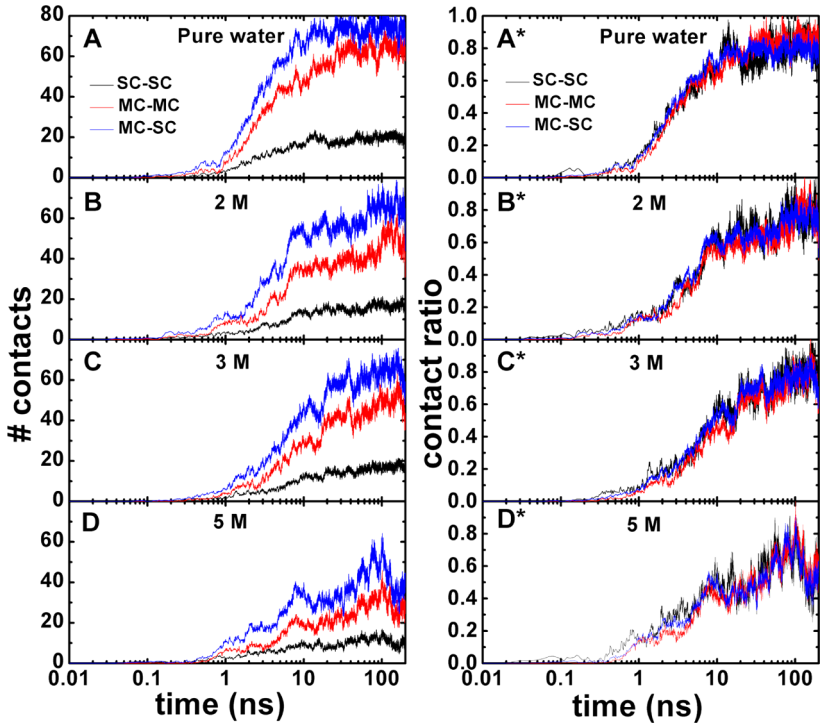


**Figure 5.** The time evolution of heavy atom contact numbers (left panels, A−D) and reduced contact ratios (right panels, A*−D*) of mc−mc (red), sc−sc (black), and mc−sc (blue), in four various urea concentrations: (A and A*) 0.0, (B and B*) 2.0, (C and C*) 3.0, and (D and D*) 5.0 M. The reduced contact ratio is defined as the percentage of the instant contact number divided by its maximum value throughout the simulation time.

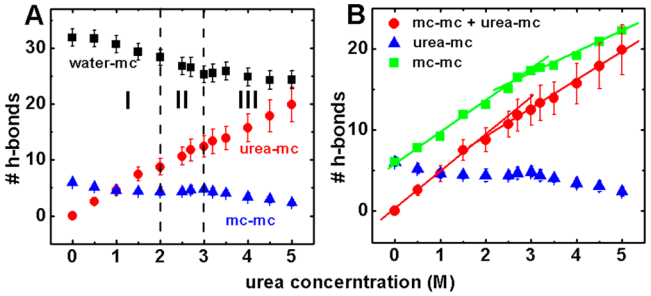


**Figure 6.** Hydrogen bonds number (50−200 ns) with the change of urea concentrations: (A) Three individual components, including mainchain-mainchain (mc−mc, blue), water−main chain (water−mc, black), and urea−main chain (urea−mc, red). (B) Number comparison between the total "stretched" hydrogen bonds (green) and the two composing elements, urea−mc (red) and mc−mc hydrogen bonds (blue). The error bars are the standard errors about the means.

are usually easier to occupy the hydrogen bonding sites than another spatially separated peptide. In regimes I and III of the urea concentration, the increment of the "stretched" hydrogen bonds is slower than that of the urea−mc hydrogen bonds (see Figure 6B). Even though the NFGAIL peptides become extended, the urea molecules accumulated in the FSS in general suppress the aggregation of the NFGAIL peptides and the formation of the $\beta$-sheet.

The increment curves of both the "stretched" and urea−mc hydrogen bonds exhibit nonlinearity with the change of the urea concentration. For the total "stretched" hydrogen bonds, the crossover from a faster to a slower increase occurs near 3.0 M whereas for the urea−mc hydrogen bonds, such a crossover occurs near 2.0 M, as shown in Figure 6B. In regime II of the urea concentration (2.0−3.0 M), the increment curve slope of the "stretched" hydrogen bonds is relatively larger than that of the urea−mc hydrogen bonds. Consequently, a slight aggregation enhancement emerges in regime II. This nonmonotonic behavior might be due to the selective accumulation of urea for different amino acids. At low urea concentrations (regime I), the urea molecules are accumulated in the FSS of residues with strong dispersion interactions, such as Phe and Ile, which are hydrophobic,[40,52] so that peptides can be largely extended as the urea concentration increases. At moderate urea concentrations (regime II), the urea molecules start to form hydrogen bonds with all the residues so that the urea−mc hydrogen bond increment slows down. The NFGAIL peptides can however still be largely extended and the increasing open hydrogen binding sites in turn promote the formation of the $\beta$-sheet. As the urea concentration further increases (regime III), the accumulated urea molecules in the FSS gradually saturate the hydrogen binding sites and eventually hinder the aggregation of peptides.

Overall, the total "stretched" hydrogen bonds are facilitated by the increment of urea molecules while the competition between the urea−mc and mc−mc hydrogen bonds leads to the nonmonotonic aggregation behavior of the NFGAIL peptides.

**Time Evolution of Aggregation Process.** To further understand the competing mechanism of the aggregation process, we explore the time evolution of different hydrogen bonds. The results from four typical urea concentrations (0.0, 2.0, 3.0, and 5.0 M) are plotted in Figure 7. In the pure water, four random-coil peptides are spatially separated initially, each surrounded by water molecules. The thermal fluctuations allow two peptides to get close so that water molecules in-between them are expelled for breaking water−mc hydrogen bonds. The water−mc hydrogen bond number decreases around 0.5 ns, initiating the peptide aggregation process. The two originally separated monomers grow into a larger oligomer but with a low


dx.doi.org/10.1021/jp407776e | J. Phys. Chem. B 2014, 118, 48−57

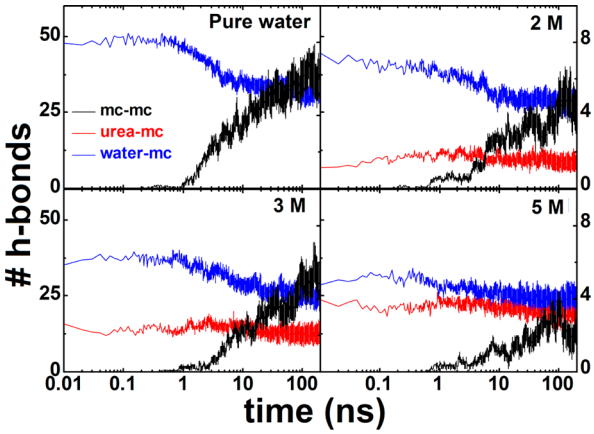


**Figure 7.** Time evolution of the hydrogen bonds numbers of mc−mc (black), water−mc (blue), and urea−mc (red) in four various urea concentrations: (A) 0.0 M, (B) 2.0 M, (C) 3.0 M, and (D) 5.0 M. For each panel, the water−mc and urea−mc hydrogen bonds refer to the left axis whereas the mc−mc hydrogen bonds refer to the right axis.

ordered structure. With a subsequent large-scale conformational fluctuation, the oligomer starts to develop mc−mc hydrogen bonds between dangling hydrogen bonding donors and acceptors. This conformational fluctuation is also reflected by the sudden change in the mc−mc heavy atom contact number (see Figure 5A). A fast growth of mc−mc hydrogen bonds is delayed until 1.0 ns. The conformational fluctuation of peptides can squeeze hydrogen-bonded water molecules out of the FSS of mainchains, thus promoting the further increase of mc−mc hydrogen bonds. After 50 ns, an ordered oligomer starts to be formed, and the water−mc and mc−mc hydrogen bond numbers approach their equilibrium values.

In urea solutions, urea molecules form additional hydrogen bonds with peptide mainchains and affect the time evolution of the peptide aggregation. From results shown in Figure 7B−D, we find that water molecules are always quickly expelled out the FSS of mainchains around 0.5 ns in various urea solutions, similar to the behavior in the pure water. The development of mc−mc hydrogen bonds is, however, different from that in the pure water. Because of the peptide extension by urea molecules, the initialization of mc−mc hydrogen bonds can occur before 1 ns. The early growth of mc−mc hydrogen bond number is not persistent but can first reach a very small plateau (<0.5) around 1 ns, hindered by the competition with urea−mc hydrogen bonds. In the same time, urea molecules can take over the hydrogen bonding sites originally occupied by water molecules, and form more hydrogen bonds with mainchains during this early stage of the peptide aggregation. After large-scale conformational fluctuations (see kinks around 1 ns for mc−mc heavy atom contact numbers in Figures 5B−D), peptide mainchains are adjusted to associate more efficiently. Urea molecules start to be expelled out of the FSS and the urea−mc hydrogen bond number decreases. The growth of mc−mc hydrogen bonds becomes accelerated after 2 ns and this "starting time" in general increases with the urea concentration. Unlike the case in the pure water, more conformational fluctuations can still be needed in the urea solutions for the final development of the $\beta$-sheet. Thus, we find that urea affect the time evolution of the aggregation process by two opposite mechanisms. On one hand, urea molecules can extend NFGAIL peptides and allow mc−mc hydrogen bonds to be initialized earlier. On the other hand, the intimate hydrogen bonds between urea and peptide mainchains require larger-scale conformational fluctuations to expel urea molecules out of the FSS so that the consistent development of mc−mc hydrogen bonds is delayed. We also calculate the radial distribution functions $g(r)$ between the carbonyl oxygen atoms of urea and the backbone amide hydrogen atoms in the first 50 ns and the final 150 ns (see Figure S2 in the Supporting Information) for the simulations at 2, 3, and 5 M urea. For the first peak for $g(r)$ associated with the FSS, its position is almost unchanged but its height decreases with time, indicating expel of urea molecules and destroy of urea−mc hydrogen bonds by the larger-scale conformational fluctuations of oligomers.

## CONCLUSIONS

In this paper, we study the aggregation process of four NFGAIL hexapeptides in aqueous urea solution by large-scale all-atom MD simulations. To explore the urea influence in detail, we select 13 different urea concentrations over a broad range from 0.0 to 5.0 M. Three parameters, including the number of hydrogen bonds, the contact number of heavy atoms, and the radius of gyration, are calculated from our MD simulations to describe the aggregation process. All the three parameters from the long-time average (50−200 ns) exhibit nonmonotonic dependences with the change of the urea concentration. Three concentration regimes, I (0.0−2.0 M), II (2.0−3.0 M), and III (>3.0 M) can be introduced to characterize the nonmonotonic aggregation behavior. The increment of urea molecules suppresses the peptide aggregation in regimes I and III, while a weak urea-enhanced aggregation is observed in regime II.

To further understand the underlying mechanism, we separate the heavy atom contact number and the hydrogen bond number to identify contributions of different factors. The equilibrium heavy atom contacts between mainchains (mc−mc), between side chains (sc−sc), and between mainchains and side chains (mc−sc) behave similarly as the urea concentration increases. The strong correlation of mainchains and side chains is further demonstrated by the similarity in the time evolution of the three reduced contact ratios (mc−mc, mc−sc, and mc−sc). The spatial adjustment of mainchains, jointed with that of side chains, is a key factor for the aggregation process of forming ordered $\beta$-sheet.

The competition among hydrogen bonds formed between water and mainchains (water−mc), between urea and mainchains (urea−mc), and between mainchains (mc−mc) determines the time evolution of the aggregation process as well as the final structure of the oligomer. The water−mc hydrogen bonds prefer a random coil structure for peptides so that the aggregation is initialized after water molecules expelled out of the FSS, which occurs around 0.5 ns. Subsequent conformational fluctuations are required to adjust mainchains and form mc−mc hydrogen bonds. In the pure water, mc−mc hydrogen bonds quickly grow after 1 ns. In the urea solutions, more extended peptides allow an earlier appearance of mc−mc hydrogen bonds (<1 ns), but the competition with urea−mc hydrogen bonds slows down the conformational fluctuations and the consistent growth is delayed. The two opposite forces of urea also affect the equilibrium structure. The sum of urea−mc and mc−mc hydrogen bonds at long times consistently increases with the urea concentration, reflecting the stretchiness increment by urea molecules. Because of the saturation at high urea concentrations, both the urea−mc and the total "stretched" (urea−mc + mc−mc) hydrogen bond numbers are nonlinear functions of the urea concentration. Interestingly,


dx.doi.org/10.1021/jp407776e | J. Phys. Chem. B 2014, 118, 48−57

the crossover from a faster to a slower increase occurs at different urea concentrations and this discrepancy leads to the nonmonotonic aggregation behavior and a weak enhancement for the poly peptide aggregation at moderate urea concentrations.

## ■ ASSOCIATED CONTENT

### Supporting Information

Some representative snapshots of oligomers in simulations at 3 and 5 M urea and radial distribution functions between the carbonyl oxygen atoms of urea and the backbone amide hydrogen for the simulations at 2, 3, and 5 M urea. This material is available free of charge via the Internet at http://pubs.acs.org.

## ■ AUTHOR INFORMATION


### Corresponding Authors

*E-mail: (J.W.) jianlanwu@zju.edu.cn.
*E-mail: (Z.Y.) jzx@zju.edu.cn.

### Author Contributions

†These authors contributed equally


### Notes

The authors declare no competing financial interest.

## ■ ACKNOWLEDGMENTS

We thank Drs. Weifeng Li and Peng Xiu for their very constructive discussions. This work was supported by grants from Research Fund for the Doctoral Program of Higher Education of China (Grant No. J20120102), the National Science Foundation of China (Grant Nos. 21173185 and 30870593), and the Fundamental Research Funds for the Central Universities in China (Grant No. 2011QNA3005), and the KYLIN-I Supercomputer in Institute for Fusion Theory and Simulation, Zhejiang University. Z.Y. is partially supported by the China Postdoctoral Science Foundation (Grant No. 2012M511351). R.Z. acknowledges the financial support from the IBM BlueGene Science Program.

## ■ REFERENCES


(1) Westermark, P.; Wernstedt, C.; Obrien, T. D.; Hayden, D. W.; Johnson, K. H. Islet Amyloid in Type 2 Human Diabetes Mellitus and Adult Diabetic Cats Contains a Novel Putative Polypeptide Hormone. *Am. J. Pathol.* **1987**, *127*, 414−417.

(2) Hoppener, J. W. M.; Ahren, B.; Lips, C. J. M. Islet Amyloid and Type 2 Diabetes Mellitus. *N. Engl. J. Med.* **2000**, *343*, 411−419.

(3) Lambert, M. P.; Barlow, A. K.; Chromy, B. A.; Edwards, C.; Freed, R.; Liosatos, M.; Morgan, T. E.; Rozovsky, I.; Trommer, B.; Viola, K. L.; et al. Diffusible, Nonfibrillar Ligands Derived From $Ab_{1-42}$ are Potent Central Nervous System Neurotoxins. *Proc. Natl. Acad. Sci. U.S.A.* **1998**, *95*, 6448−6453.

(4) Selkoe, D. J. Alzheimer's Disease: Genes, Proteins, and Therapy. *Physiol. Rev.* **2001**, *81*, 741−766.

(5) Hardy, J.; Selkoe, D. J. The Amyloid Hypothesis of Alzheimer's Disease: Progress and Problems on the Road to Therapeutics. *Science* **2002**, *297*, 353−356.

(6) Oyster, C. W. *The Human Eye: Structure and Function*; Sinauer Associates: Sunderland, MA, 1999.

(7) Khemtemourian, L.; Killian, J. A.; Hoppener, J. W. M.; Engel, M. F. M. Recent Insights in Islet Amyloid Polypeptide-Induced Membrane Disruption and Its Role in beta-Cell Death in Type 2 Diabetes Mellitus. *Exp. Diabetes. Res.* **2008**, 421287.

(8) Pastor, M. T.; Kummerer, N.; Schubert, V.; Esteras-Chopo, A.; Dotti, C. G.; de la Paz, M. L.; Serrano, L. Amyloid Toxicity is Independent of Polypeptide Sequence, Length and Chirality. *J. Mol. Biol.* **2008**, *375*, 695−707.

(9) Engel, M. F. M. Membrane Permeabilization by Islet Amyloid Polypeptide. *Chem. Phys. Lipids* **2009**, *160*, 1−10.

(10) Last, N. B.; Rhoades, E.; Miranker, A. D. Islet Amyloid Polypeptide Demonstrates a Persistent Capacity to Disrupt Membrane Integrity. *Proc. Natl. Acad. Sci. U.S.A.* **2011**, *108*, 9460−9465.

(11) Janson, J.; Ashley, R. H.; Harrison, D.; McIntyre, S.; Butler, P. C. The Mechanism of Islet Amyloid Polypeptide Toxicity is Membrane Disruption by Intermediate-Sized Toxic Amyloid Particles. *Diabetes* **1999**, *48*, 491−498.

(12) Bucciantini, M.; Giannoni, E.; Chiti, F.; Baroni, F.; Formigli, L.; Zurdo, J. S.; Taddei, N.; Ramponi, G.; Dobson, C. M.; Stefani, M. Inherent Toxicity of Aggregates Implies a Common Mechanism for Protein Misfolding Diseases. *Nature* **2002**, *416*, 507−511.

(13) Sparr, E.; Engel, M. F. M.; Sakharov, D. V.; Sprong, M.; Jacobs, J.; de Kruijff, B.; Hoppener, J. W. M.; Killian, J. A. Islet Amyloid Polypeptide-Induced Membrane Leakage Involves Uptake of Lipids by Forming Amyloid Fibers. *FEBS Lett.* **2004**, *577*, 117−120.

(14) Engel, M. F. M.; Khemtemourian, L.; Kleijer, C. C.; Meeldijk, H. J. D.; Jacobs, J.; Verkleij, A. J.; de Kruijff, B.; Killian, J. A.; Hoppener, J. W. M. Membrane Damage by Human Islet Amyloid Polypeptide Through Fibril Growth at the Membrane. *Proc. Natl. Acad. Sci. U.S.A.* **2008**, *105*, 6033−6038.

(15) Laganowsky, A.; Liu, C.; Sawaya, M. R.; Whitelegge, J. P.; Park, J.; Zhao, M. L.; Pensalfini, A.; Soriaga, A. B.; Landau, M.; Teng, P. K.; et al. Atomic View of a Toxic Amyloid Small Oligomer. *Science* **2012**, *335*, 1228−1231.

(16) Thirumalai, D.; Klimov, D. K.; Dima, R. I. Emerging Ideas on the Molecular Basis of Protein and Peptide Aggregation. *Curr. Opin. Struct. Biol.* **2003**, *13*, 146−159.

(17) Pace, C. N. Determination and Analysis of Urea and Guanidine Hydrochloride Denaturation Curves. *Methods Enzymol.* **1986**, *131*, 266−280.

(18) Frank, H. S.; Franks, F. Structural Approach to Solvent Power of Water for Hydrocarbons - Urea as a Structure Breaker. *J. Chem. Phys.* **1968**, *48*, 4746−4757.

(19) Wetlaufer, D. B.; Coffin, R. L.; Malik, S. K.; Stoller, L. Nonpolar Group Participation in the Denaturation of Proteins by Urea and Guanidinium Salts. Model Compound Studies. *J. Am. Chem. Soc.* **1964**, *86*, 508−514.

(20) Hammes, G. G.; Schimmel, P. R. An Investigation of Water-Urea and Water-Urea-Polyethylene Glycol Interactions. *J. Am. Chem. Soc.* **1967**, *89*, 442−446.

(21) Chen, X.; Sagle, L. B.; Cremer, P. S. Urea Orientation at Protein Surfaces. *J. Am. Chem. Soc.* **2007**, *129*, 15104−15105.

(22) Sagle, L. B.; Zhang, Y. J.; Litosh, V. A.; Chen, X.; Cho, Y.; Cremer, P. S. Investigating the Hydrogen-Bonding Model of Urea Denaturation. *J. Am. Chem. Soc.* **2009**, *131*, 9304−9310.

(23) Bennion, B. J.; Daggett, V. The Molecular Basis for the Chemical Denaturation of Proteins by Urea. *Proc. Natl. Acad. Sci. U.S.A.* **2003**, *100*, 5142−5147.

(24) England, J. L.; Pande, V. S.; Haran, G. Chemical Denaturants Inhibit the Onset of Dewetting. *J. Am. Chem. Soc.* **2008**, *130*, 11854−11855.

(25) Yang, L. J.; Gao, Y. Q. Effects of Cosolvents on the Hydration of Carbon Nanotubes. *J. Am. Chem. Soc.* **2010**, *132*, 842−848.

(26) Wei, H. Y.; Fan, Y. B.; Gao, Y. Q. Effects of Urea, Tetramethyl Urea, and Trimethylamine N-Oxide on Aqueous Solution Structure and Solvation of Protein Backbones: A Molecular Dynamics Simulation Study. *J. Phys. Chem. B* **2010**, *114*, 557−568.

(27) Caflisch, A.; Karplus, M. Structural Details of Urea Binding to Barnase: a Molecular Dynamics Analysis. *Struct. Fold. Des.* **1999**, *7*, 477−488.

(28) Caballero-Herrera, A.; Nordstrand, K.; Berndt, K. D.; Nilsson, L. Effect of Urea on Peptide Conformation in Water: Molecular Dynamics and Experimental Characterization. *Biophys. J.* **2005**, *89*, 842−857.

(29) Robinson, D. R.; Jencks, W. P. Effect of Compounds of Urea-Guanidinium Class on Activity Coefficient of Acetyltetraglycine Ethyl Ester and Related Compounds. *J. Am. Chem. Soc.* **1965**, *87*, 2462−2470.
(30) Makhatadze, G. I.; Privalov, P. L. Protein Interactions With Urea and Guanidinium Chloride - A Calorimetric Study. *J. Mol. Biol.* **1992**, *226*, 491−505.
(31) Sharp, K. A.; Madan, B.; Manas, E.; Vanderkooi, J. M. Water Structure Changes Induced by Hydrophobic and Polar Solutes Revealed by Simulations and Infrared Spectroscopy. *J. Chem. Phys.* **2001**, *114*, 1791−1796.
(32) Auton, M.; Holthauzen, L. M. F.; Bolen, D. W. Anatomy of Energetic Changes Accompanying Urea-Induced Protein Denaturation. *Proc. Natl. Acad. Sci. U.S.A.* **2007**, *104*, 15317−15322.
(33) Lim, W. K.; Rosgen, J.; Englander, S. W. Urea, But not Guanidinium, Destabilizes Proteins by Forming Hydrogen Bonds to the Peptide Group. *Proc. Natl. Acad. Sci. U.S.A.* **2009**, *106*, 2595−2600.
(34) Klimov, D. K.; Straub, J. E.; Thirumalai, D. Aqueous Urea Solution Destabilizes $Ab_{16-22}$ Oligomers. *Proc. Natl. Acad. Sci. U.S.A.* **2004**, *101*, 14760−14765.
(35) Mountain, R. D.; Thirumalai, D. Molecular Dynamics Simulations of End-to-End Contact Formation in Hydrocarbon Chains in Water and Aqueous Urea Solution. *J. Am. Chem. Soc.* **2003**, *125*, 1950−1957.
(36) O'Brien, E. P.; Dima, R. I.; Brooks, B.; Thirumalai, D. Interactions between Hydrophobic and Ionic Solutes in Aqueous Guanidinium Chloride and Urea Solutions: Lessons for Protein Denaturation Mechanism. *J. Am. Chem. Soc.* **2007**, *129*, 7346−7353.
(37) Berteotti, A.; Barducci, A.; Parrinello, M. Effect of Urea on the beta-Hairpin Conformational Ensemble and Protein Denaturation Mechanism. *J. Am. Chem. Soc.* **2011**, *133*, 17200−17206.
(38) Canchi, D. R.; Paschek, D.; Garcia, A. E. Equilibrium Study of Protein Denaturation by Urea. *J. Am. Chem. Soc.* **2010**, *132*, 2338−2344.
(39) Canchi, D. R.; Garcia, A. E. Backbone and Side-Chain Contributions in Protein Denaturation by Urea. *Biophys. J* . **2011**, *100*, 1526−1533.
(40) Stumpe, M. C.; Grubmuller, H. Interaction of Urea with Amino Acids: Implications for Urea-Induced Protein Denaturation. *J. Am. Chem. Soc.* **2007**, *129*, 16126−16131.
(41) Stumpe, M. C.; Grubmuller, H. Polar or Apolar-The Role of Polarity for Urea-Induced Protein Denaturation. *PLoS Comput. Biol.* **2008**, *4*, e1000221.
(42) Lee, M. E.; van der Vegt, N. F. A. Does Urea Denature Hydrophobic Interactions? *J. Am. Chem. Soc.* **2006**, *128*, 4948−4949.
(43) Hua, L.; Zhou, R. H.; Thirumalai, D.; Berne, B. J. Urea Denaturation by Stronger Dispersion Interactions with Proteins than Water Implies a 2-Stage Unfolding. *Proc. Natl. Acad. Sci. U.S.A.* **2008**, *105*, 16928−16933.
(44) Li, W.; Zhou, R.; Mu, Y. Salting Effects on Protein Components in Aqueous NaCl and Urea Solutions: Toward Understanding of Urea-Induced Protein Denaturation. *J. Phys. Chem. B* **2012**, *116*, 1446−1451.
(45) Zangi, R.; Zhou, R. H.; Berne, B. J. Urea's Action on Hydrophobic Interactions. *J. Am. Chem. Soc.* **2009**, *131*, 1535−1541.
(46) Das, P.; Zhou, R. H. Urea-Induced Drying of Carbon Nanotubes Suggests Existence of a Dry Globule-like Transient State During Chemical Denaturation of Proteins. *J. Phys. Chem. B* **2010**, *114*, 5427−5430.
(47) Xiu, P.; Yang, Z. X.; Zhou, B.; Das, P.; Fang, H. P.; Zhou, R. H. Urea-Induced Drying of Hydrophobic Nanotubes: Comparison of Different Urea Models. *J. Phys. Chem. B* **2011**, *115*, 2988−2994.
(48) Zhou, R. H.; Li, J. Y.; Hua, L.; Yang, Z. X.; Berne, B. J. Comment on "Urea-Mediated Protein Denaturation: A Consensus View". *J. Phys. Chem. B* **2011**, *115*, 1323−1326.
(49) Das, A.; Mukhopadhyay, C. Urea-Mediated Protein Denaturation: A Consensus View. *J. Phys. Chem. B* **2009**, *113*, 12816−12824.
(50) Jha, S. K.; Udgaonkar, J. B. Direct Evidence for a Dry Molten Globule Intermediate During the Unfolding of a Small Protein. *Proc. Natl. Acad. Sci. U.S.A.* **2009**, *106*, 12289−12294.
(51) Wallqvist, A.; Covell, D. G.; Thirumalai, D. Hydrophobic Interactions in Aqueous Urea Solutions with Implications for the Mechanism of Protein Denaturation. *J. Am. Chem. Soc.* **1998**, *120*, 427−428.
(52) Yang, Z. X.; Xiu, P.; Shi, B. Y.; Hua, L.; Zhou, R. H. Coherent Microscopic Picture for Urea-Induced Denaturation of Proteins. *J. Phys. Chem. B* **2012**, *116*, 8856−8862.
(53) Candotti, M.; Esteban-Martin, S.; Salvatella, X.; Orozco, M. Toward an Atomistic Description of the Urea-Denatured State of Proteins. *Proc. Natl. Acad. Sci. U.S.A.* **2013**, *110*, 5933−5938.
(54) Hamada, D.; Dobson, C. M. A Kinetic Study of *b*-Lactoglobulin Amyloid Fibril Formation Promoted by Urea. *Protein Sci.* **2002**, *11*, 2417−2426.
(55) Massi, F.; Straub, J. E. Energy Landscape Theory for Alzheimer's Amyloid *b*-peptide Fibril Elongation. *Proteins* **2001**, *42*, 217−229.
(56) Guo, Z. Y.; Thirumalai, D. Kinetics of Protein folding: Nucleation Mechanism, Time Scales, and Pathways. *Biopolymers* **1995**, *36*, 83−102.
(57) Lindahl, E.; Hess, B.; van der Spoel, D. GROMACS 3.0: A Package for Molecular Simulation and Trajectory Analysis. *J. Mol. Model.* **2001**, *7*, 306−317.
(58) Humphrey, W.; Dalke, A.; Schulten, K. VMD: Visual Molecular Dynamics. *J. Mol. Graph.* **1996**, *14*, 33−38.
(59) Jorgensen, W. L.; Maxwell, D. S.; Tirado-Rives, J. Development and Testing of the OPLS All-Atom Force Field on Conformational Energetics and Properties of Organic Liquids. *J. Am. Chem. Soc.* **1996**, *118*, 11225−11236.
(60) Choudhury, N.; Pettitt, B. M. On the Mechanism of Hydrophobic Association of Nanoscopic Solutes. *J. Am. Chem. Soc.* **2005**, *127*, 3556−3567.
(61) Duffy, E. M.; Severance, D. L.; Jorgensen, W. L. Urea: Potential Functions, log P, and Free Energy of Hydration. *Isr. J. Chem.* **1993**, *33*, 323−330.
(62) Smith, L. J.; Berendsen, H. J. C.; van Gunsteren, W. F. Computer Simulation of Urea-Water Mixtures: A Test of Force Field Parameters for Use in Biomolecular Simulation. *J. Phys. Chem. B* **2004**, *108*, 1065−1071.
(63) Hess, B.; Bekker, H.; Berendsen, H. J. C.; Fraaije, J. LINCS: A Linear Constraint Solver for Molecular Simulations. *J. Comput. Chem.* **1997**, *18*, 1463−1472.
(64) Miyamoto, S.; Kollman, P. A. Settle:An Analytical Version of the SHAKE and RATTLE Algorithm for Rigid Water Models. *J. Comput. Chem.* **1992**, *13*, 952−962.
(65) Berendsen, H. J. C.; Postma, J. P. M.; Vangunsteren, W. F.; Dinola, A.; Haak, J. R. Molecular Dynamics with Coupling to an External Bath. *J. Chem. Phys.* **1984**, *81*, 3684−3690.
(66) Nielsen, J. T.; Bjerring, M.; Jeppesen, M. D.; Pedersen, R. O.; Pedersen, J. M.; Hein, K. L.; Vosegaard, T.; Skrydstrup, T.; Otzen, D. E.; Nielsen, N. C. Unique Identification of Supramolecular Structures in Amyloid Fibrils by Solid-State NMR Spectroscopy. *Angew. Chem., Int. Ed.* **2009**, *48*, 2118−2121.
(67) Eleftheriou, M.; Germain, R. S.; Royyuru, A. K.; Zhou, R. H. Thermal Denaturing of Mutant Lysozyme with Both the OPLSAA and the CHARMM Force Fields. *J. Am. Chem. Soc.* **2006**, *128*, 13388−13395.
(68) Huang, X. H.; Hagen, M.; Kim, B.; Friesner, R. A.; Zhou, R. H.; Berne, B. J. Replica Exchange with Solute Tempering: Efficiency in Large Scale Systems. *J. Phys. Chem. B* **2007**, *111*, 5405−5410.
(69) Li, X.; Li, J. Y.; Eleftheriou, M.; Zhou, R. H. Hydration and Dewetting Near Fluorinated Superhydrophobic Plates. *J. Am. Chem. Soc.* **2006**, *128*, 12439−12447.
(70) Zhou, R. H.; Berne, B. J.; Germain, R. The Free Energy Landscape for *b* Hairpin Folding in Explicit Water. *Proc. Natl. Acad. Sci. U.S.A.* **2001**, *98*, 14931−14936.

(71) Zhou, R. H.; Huang, X. H.; Margulis, C. J.; Berne, B. J. Hydrophobic Collapse in Multidomain Protein Folding. *Science* **2004**, *305*, 1605−1609.
(72) Mu, Y. G.; Nguyen, P. H.; Stock, G. Energy Landscape of a Small Peptide Revealed by Dihedral Angle Principal Component Analysis. *Proteins* **2005**, *58*, 45−52.
(73) Nguyen, P. H.; Stock, G.; Mittag, E.; Hu, C. K.; Li, M. S. Free Energy Landscape and Folding Mechanism of a *b*-Hairpin in Explicit Water: A Replica Exchange Molecular Dynamics Study. *Proteins* **2005**, *61*, 795−808.
(74) Ichiye, T.; Karplus, M. Collective Motions in Proteins: A Covariance Analysis of Atomic Fluctuations in Molecular Dynamics and Normal Mode Simulations. *Proteins* **1991**, *11*, 205−217.
(75) Garcia, A. E. Large-Amplitude Nonlinear Motions in Proteins. *Phys. Rev. Lett.* **1992**, *68*, 2696−2699.
(76) Amadei, A.; Linssen, A. B. M.; Berendsen, H. J. C. Essential Dynamics of Proteins. *Proteins* **1993**, *17*, 412−425.
(77) Kitao, A.; Hirata, F.; Go, N. The Effects of Solvent on the Conformation and the Collective Motions of Protein: Normal Mode Analysis and Molecular Dynamics Simulations of Melittin in Water and in Vacuum. *Chem. Phys.* **1991**, *158*, 447−472.
(78) Wu, C.; Lei, H. X.; Duan, Y. Formation of Partially Ordered Oligomers of Amyloidogenic Hexapeptide (NFGAIL) in Aqueous Solution Observed in Molecular Dynamics Simulations. *Biophys. J.* **2004**, *87*, 3000−3009.
(79) Li, W. F.; Zhang, J.; Su, Y.; Wang, J.; Qin, M.; Wang, W. Effects of Zinc Binding on the Conformational Distribution of the Amyloid-*b* Peptide Based on Molecular Dynamics Simulations. *J. Phys. Chem. B* **2007**, *111*, 13814−13821.
(80) Shi, B. Y.; Zhou, B.; Cai, Z. W.; Xiu, P.; Yang, Z. X. Molecular Mechanism of the Early Stage of Amyloidogenic Hexapeptides (NFGAIL) Aggregation. *Commun. Theor. Phys.* **2013**, *60*, 515.